OFFICE OF NAVAL RESEARCH

Grant N00014-90-J-1971

R&T Code 4131001 phy

Technical Report No. 4

High Resolution Spectroscopy of 1,2-Difluoroethane in a Molecular Beam: A Case Study of Vibrational Mode-Coupling

by

Steven W. Mork, C. Cameron Miller, and Laura A. Philips

Accepted for Publication
in the
Journal of Chemical Physics

Cornell University
Department of Chemistry
Ithaca, NY 14853-1301

May 29, 1992

HIGH RESOLUTION SPECTROSCOPY OF 1,2-DIFLUOROETHANE IN A MOLECULAR BEAM: A CASE STUDY OF VIBRATIONAL MODE-COUPLING

Steven W. Mork, C. Cameron Miller, Laura A. Philips
Department of Chemistry, Cornell University, Ithaca, New York, 14853-1301

Abstract

The high resolution infrared spectrum of 1,2-difluoroethane (DFE) in a molecular beam has been obtained over the 2978-2996 cm^{-1} spectral region. This region corresponds to the symmetric combination of asymmetric C-H stretches in DFE. Observed rotational fine structure indicates that this C-H stretch is undergoing vibrational mode coupling to a single dark mode. The dark mode is split by approximately 19 cm^{-1} due to tunneling between the two identical gauche conformers. The mechanism of the coupling is largely anharmonic with a minor component of B/C plane Coriolis coupling. Effects of centrifugal distortion along the molecular A-axis are also observed. Analysis of the fine structure identifies the dark state as being composed of C-C torsion, CCF bend and CH_2 rock. Coupling between the C-H stretches and the C-C torsion is of particular interest because DFE has been observed to undergo vibrationally induced isomerization from the gauche to trans conformer upon excitation of the C-H stretch.

Introduction

An understanding of vibrational interactions can provide insight into molecular behavior, from chemical reactions to intramolecular vibrational energy redistribution (IVR). Molecular vibrations have been the focus of both theoretical and experimental studies aimed at understanding the physical effects of vibrational excitation. Spectroscopy has been a powerful tool for driving theoretical models of vibrational energy levels. As spectroscopic methods have attained increasingly higher resolution, simple models

for calculating vibrational energy levels, such as normal modes or local modes, have proven insufficient to interpret experimental data. For instance, splittings in rotational fine structure due to coupling between different normal modes have been observed through the development of high resolution U.V. and I.R. spectroscopic techniques. Such vibrational mode coupling provides insight into molecular potential energy surfaces.

Vibrational mode-coupling has been observed spectroscopically in both the ground and the excited electronic potential surfaces. Pyrazine, for example, has been studied extensively using rotationally resolved electronic spectroscopy, providing a wealth of information about vibrational interactions and energy flow in pyrazine's excited electronic state.[1] Interesting vibrational behavior is also present in the electronic ground states of molecules. de Souza, Kaun and Perry used infrared spectroscopy to study the vibrational mode coupling in the electronic ground state of 1-butyne.[2] Subsequent studies followed in an effort to extract the abundance of information in the rotationally resolved infrared spectrum of 1-butyne[3] as well as molecules such as ethanol[4] and 2-fluoroethanol (2FE).[5,6] The present study employs high resolution infrared spectroscopy in a molecular beam to explore vibrational mode coupling in 1,2-difluoroethane (DFE).

DFE is unique among 1,2-dihalogenoethanes, XCH_2CH_2X, and as a result, has been extensively studied both theoretically[7-14] and experimentally[15-24]. The most stable geometry for DFE has been experimentally determined to be a gauche conformation with an FCCF

dihedral angle of approximately 72°.[16,18,24] DFE is the only 1,2-dihalogenoethane in which the gauche conformer is more stable than the trans conformer.[25] Theoretical calculations have difficulty accounting for the stability of the gauche form of DFE.[8,9] The numerous qualitative explanations for the stability of the gauche conformer fall into the general heading known as the "Gauche Effect".[26]

DFE also exhibits dynamics that are different form other 1,2-dihalogenoethanes. DFE has been observed to undergo a vibrationally induced isomerization from the gauche to the trans conformer upon excitation of its C-H stretches. This photoisomerization was observed for DFE trapped in low temperature Xe and Kr matrices.[19,27] Although the other 1,2-dihalogenoethanes do not exhibit this photoisomerization, several molecules have been observed to undergo similar photoisomerization reactions including 2-fluoroethanol (2FE), ethylene glycol, 2-aminoethanol and 2-fluoroethylamine.[27-30] The mechanisms for these reactions are not well understood. The photoisomerization of 2FE has been studied extensively[28-30] and two possible mechanisms have been proposed. The first mechanism involves random vibrational energy redistribution within the molecule as a result of interactions with the surrounding matrix environment.[28] The second mechanism involves selective vibrational mode coupling between the excited vibration and vibrations critical to isomerization.[29] Mode coupling in this second mechanism provides a specific pathway for intramolecular energy redistribution. The photoisomerization of DFE is also thought

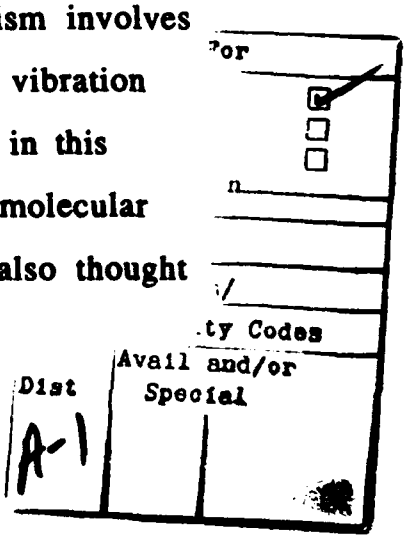

to occur by one of these mechanisms. For DFE to isomerize via selective vibrational mode coupling, the C-H stretch must be coupled primarily to the C-C torsional mode. High resolution spectroscopy provides a tool to measure the extent of vibrational mode-coupling between these different vibrations.

The research presented in this paper employs high resolution infrared spectroscopy in a molecular beam to probe the rovibrational states of DFE in an effort to investigate vibrational interactions within the molecule. Vibrational mode coupling between the C-H stretch and the C-C torsion is of particular interest as the torsion is the photoisomerization reaction coordinate. A high resolution infrared spectral analysis of the C-H stretch is presented here.

Experimental

The DFE spectra were collected using a color-center laser, supersonic molecular beam and optothermal detection, as described in detail elsewhere.[6] The experimental apparatus will be described briefly here.

The color-center laser was pumped with an argon-ion pumped dye laser and provided a tunable infrared laser beam with a spectral resolution of approximately 7 MHz. The frequency of the infrared beam was scanned over the 2995-2975 cm^{-1} spectral region, corresponding to the frequency of the symmetric combination of asymmetric C-H stretches in DFE (MOPAC calculation). The infrared

beam was continually monitored throughout the scan using a PbSe power detector, 750 MHz etalon and 7.5 GHz spectrum analyzer. These devices allowed for detection and correction of laser power fluctuations as well as nonlinearities in the frequency scan, as described elsewhere.[6] The laser beam was mechanically chopped at 168 Hz, allowing for phase sensitive detection using a lock-in detector. The laser was focused onto the molecular beam and then reflected through the molecular beam approximately 40 times using parallel mirrors. Multipassing the laser through the molecular beam decreased the spectral resolution to roughly 12 MHz but increased the signal-to-noise by approximately a factor of 8.

The supersonic molecular beam was formed by expanding a mixture of helium gas and DFE through a 50 μm pinhole into the first of three differentially pumped vacuum chambers. The center of the expansion was selected using a 500 μm skimmer located approximately 4 cm from the expansion nozzle. The molecular beam continued into the second vacuum chamber where it was crossed with the laser beam. A 10 mm aperture allowed the molecular beam to continue into the third vacuum chamber where it was monitored by a bolometer detector.

The bolometer consisted of a gallium doped silicon surface with a 2 mm by 6 mm diamond mounted on it to increase surface area. A 2 mm diameter aperture was mounted over the diamond surface. The bolometer was cooled to approximately 1.6 K using liquid helium. The signal from the bolometer was sent to the lock-in amplifier.

DFE was purchased from Flura Corporation. The sample was 99.6% pure (by G.C.) and was used without further purification. DFE was seeded into the molecular beam by flowing helium gas through several milliliters of the sample located in a stainless steel reservoir approximately 80 cm before the expansion nozzle. The helium gas pressure was maintained at 6 psig. The reservoir and sample were maintained at -45° C ± 4° using a 95.5% carbon tetrachloride/4.5% chloroform/dry ice slush.

The spectrum was assembled from individual 0.12 cm^{-1} scans, which were linearized, and intensity normalized as described elsewhere.[6] The spacing of the 750 MHz etalon was calibrated over a 15.2463 cm^{-1} region before and after each day's experiments using known acetylene transitions. The transmitted frequency markers from this etalon were used to linearize the final spectrum. A peak at 2986.23 cm^{-1}, assigned to the $7_{17} \leftarrow 7_{07}$ transition, was used to monitor bolometer sensitivity. Every 0.5 cm^{-1} the intensity of this transition and the laser power were measured. These measurements provided an indication of relative bolometer sensitivity throughout the scan. Another transition at 2986.03 cm^{-1} , corresponding to the $1_{11} \leftarrow 1_{01}$ transition, was monitored as well. Comparison of the relative intensities of these two peaks allowed us to detect changes in the rotational temperature throughout the scan.

Results and Analysis

Spectral Assignments

Spectral assignments were made by comparing a calculated spectrum with the experimental spectrum. Spectra were calculated using ten molecular and spectral parameters: 3 ground state rotational constants, 3 excited state rotational constants, 2 angles which determine the orientation of transition dipole with respect to the inertial axes of the molecule, the 0-0 transition frequency and the rotational temperature. The rotational energy levels were determined by exact diagonalization of the asymmetric top rigid rotor Hamiltonian.[31] The ground state rotational constants were held constant at literature values[32] and the remaining seven parameters were varied to optimize the fit of the calculated spectrum to the experimental spectrum. A modified simulated annealing algorithm was employed to conduct the seven dimensional fit, minimizing the difference between the calculated and experimental rotational contours.[33] The calculated spectrum found to best match the experimental rotational contour is shown with the experimental spectrum in Figure 1. The best fit was attained with a vibrational transition that is A-type and C-type in a ratio of approximately 12:88, respectively. The average rotational temperature for the contour was found to be 8.1 K. The rotational constants are presented in Table 1. The similarity between the ground and excited rotational constants implies that the excited vibrational state equilibrium geometry is similar to the geometry of the ground vibrational state.

Close inspection of the experimental spectrum revealed splittings in the rotational fine structure when compared to the calculated spectrum. The splittings consisted primarily of doublets located about single transitions in the calculated spectrum. Of the 293 assigned multiplets, there are 23 singlets, 260 doublets, and 10 triplets (see Table 2). The splittings were determined to be the result of vibrational mode coupling.

Vibrational mode coupling is a means by which rotational states in one zeroth-order vibration can combine with the rotational states in other zeroth-order vibrations. In the case of DFE, the zeroth-order vibrations are defined by the normal mode vibrations. Within the zeroth-order approximation a single bright state is defined as having a large transition probability with the ground vibrational state. The bright state for this spectrum of DFE is the C-H stretch. A dark state is defined as having negligible transition probability with the ground vibrational state and is usually composed of overtones and combinations of lower frequency vibrations. Mode coupling between the bright state and one or more dark states produces two or more rotational eigenstates in the vicinity of the zero-order bright state. Our calculated spectrum represents rovibrational transitions to the zeroth-order bright rotational states in the C-H stretch.

The experimental spectrum represents transitions to the actual molecular eigenstates of DFE. As a result, multiplets appear in the vicinity of each zeroth-order calculated peak. Quantum numbers

were assigned to the experimental multiplets using the assignments from the corresponding calculated transitions. In total, 80% of the peaks with an intensity ≥ 10% that of the most intense peak have been assigned[34]. Vibrational mode coupling was confirmed by examining transitions which terminate in identical excited states and originated in different ground states (e.g. P and R transitions to the same state). Such pairs of transitions were found to have equivalent frequency and intensity patterns. These comparisons were also used to confirm quantum number assignments to experimental peaks.

Mode-Coupling Pictures

We examined two possible vibrational mode coupling pictures in DFE. The difference between these two pictures is in the nature of the dark state coupling to the C-H stretch. The C-H stretch can be coupled to either a dark vibration containing few or no C-C torsional quanta, or to a dark vibration containing significant torsional quanta.

The torsional potential for DFE can be defined using a Fourier series expansion as follows:

$$V = (1/2)\sum_{i=1}^{3} V_i(1 - \cos(i\Theta)) \qquad \text{Eq.1}$$

The values of V_1= -740 cm^{-1}, V_2= -980 cm^{-1} and V_3= -1170 cm^{-1} where Θ= C-C torsion angle were taken from reference 16, having been chosen so as to reproduce the experimentally determined characteristics of the potential surface. The two equivalent gauche conformations for DFE are separated by a 2200 cm^{-1} barrier on this

potential surface. Tunneling splitting between the two gauche potential wells results in symmetric and antisymmetric torsional states. The splitting in the ground torsional state is very small, unresolvable even in microwave spectra.[16-18] Therefore, the ground torsional energy level is essentially degenerate. States containing significant quanta of torsion experience much larger tunnelling splitting. The magnitude of the splitting in the coupled dark state distinguishes one mode coupling picture from the other.

The first possible mode coupling picture involves a dark state containing little or no torsional quanta, and therefore the symmetric and antisymmetric dark states are essentially degenerate. The bright state consists solely of the C-H stretch fundamental so it is also degenerate. When vibrational levels are doubly degenerate, the rotational levels must also be doubly degenerate. Coupling can occur between bright and dark rotational states of like symmetry. Symmetric states, however, cannot mix with antisymmetric states. The result of coupling between two such states is shown schematically in Figure 2a. This first mode coupling picture produces four rotational eigenstates -- two doubly degenerate energy levels for each bright state rotational level. This mode coupling picture would produce an experimental rovibrational spectrum containing two transitions for each calculated transition.

The second mode coupling picture involves coupling to a dark state containing significant torsional quanta. The coupling scheme for this picture is shown in Figure 2b. Note that the symmetric and antisymmetric dark states are no longer degenerate. This vibrational

mode coupling picture produces four molecular eigenstates, each of unique energy, for each rotational bright state. The rovibrational spectrum produced with this picture would contain four peaks for each calculated zero-order transition. The two vibrational mode coupling pictures were examined in an effort to reproduce the rotational fine structure observed in the experimental spectrum.

Rotational Splittings

The doublets in the experimental rotational fine structure display intriguing splitting and intensity patterns. For example, the Q-branch transitions with K_a=0 show a decrease in doublet splitting as the energy of the excited state increases.[35] The doublet splittings decrease until the splitting cannot be resolved with our spectral resolution. At higher excited state energies, the doublet splittings are resolved once again. Throughout the variation in splitting, the relative intensities of the doublet pairs remain approximately equal. Part of the progression for K_a = 0 is shown in Figure 3. A similar trend occurs in Q-branch transitions for K_a=1 Shown in Figure 4 is a plot of the doublet splittings versus excited state energies for the K_a=0 and K_a=1 progressions. Transitions with higher K_a values display an opposite splitting behavior. The doublet splittings for higher K_a's, in general, increase and then decrease with progressively higher excited state energies. The relative intensities of the doublet pairs once again remain equal. A plot of doublet splittings versus excited state energy for the K_a=3,4,5 progressions is shown in Figure 5. This unusual splitting behavior was used to test the two mode coupling pictures described above.

Calculated Rotational Splitting

The two mode coupling pictures were examined to see which was capable of reproducing the splitting behavior observed experimentally. The mode coupling picture involving degenerate symmetric and antisymmetric dark states is discussed first. This first mode coupling picture is expected to produce two transitions for each zeroth-order transition, as observed. The bright and dark states are assumed to have slightly different rotational constants, since the equilibrium geometries for these modes will not be identical. The different rotational constants produce different rotational level spacings in the bright vibration than in the dark vibration. The different spacings bring about a tuning and detuning of bright and dark rotational levels as one progresses to higher rotational levels (see Figure 6).

As a degenerate bright rotational level approaches a degenerate dark rotational level the spacing between the two resulting eigenstate levels decreases as shown in Figure 7. The minimum eigenstate spacing occurs when the bright and dark rotational levels are degenerate. The spacing once again increases as the bright and dark levels diverge. The tuning and detuning of degenerate bright and dark rotational states can produce a general doublet splitting pattern similar to that observed in the K_a=0 and K_a=1 doublet progressions. The peak intensities within each doublet, however, are dramatically different than that observed experimentally. A calculation was performed in an attempt to

reproduce the doublet spacing and intensities as observed in the K_a=1 progression. The smallest doublet spacing observed in the Ka=1 progression was reproduced with the bright and dark levels degenerate. These peaks were equal in intensity[36] as observed experimentally. Maintaining a constant coupling matrix element, the intensities of the doublet peaks were calculated for the eigenstate spacing experimentally observed for the 1_{10} excited rotational state. Experimentally, these peaks were of equivalent intensities. The calculated doublet intensities, however, were in a ratio of 526:1. Allowing the bright state to couple to more than one dark state could not resolve these discrepancies.

The second vibrational mode coupling picture, that involving a dark state with significant torsional quanta, was also examined. As mentioned above, this picture would produce four spectrally resolvable transitions for each calculated bright state transition. Two of the four transitions are generally much more intense than the other two (see Figure 8). One of the two intense peaks corresponds to excitation of an eigenstate with predominantly symmetric bright state character while the other intense peak corresponds to excitation of an eigenstate with predominantly antisymmetric bright state character. These intense peaks are located near the frequency of the zero-order bright state transition and are as much as several orders of magnitude more intense than the smaller two transitions. It is reasonable to assume that the two smaller peaks could disappear in the baseline noise some distance from the bright state leaving only the more intense "doublet" visible.

Once again it is assumed that the bright and dark states are described by different rotational constants. As a result, the bright rotational energy level varies with respect to the position of the dark rotational levels as one increases energy as shown in Figure 6. In this coupling picture, minimal splitting occurs in the intense doublet when the bright state level is far from the dark state levels. Splitting increases as the bright state approaches a dark state level as shown in Figure 9. The parabolic splitting behavior of the experimental K_a=0 and K_a=1 progressions is reproduced by tuning the degenerate bright rotational state level between the symmetric and antisymmetric dark rotational states. Minimal splitting occurs in this parabolic splitting pattern when the bright state is midway between the dark rotational states. Moreover, the two large peaks remain nearly equal in intensity throughout this progression. The intensities calculated for the 1_{10} doublets were found to have relative intensities of 1.008:1, in excellent agreement with the experimental value.

The patterns observed for doublet progressions of higher K_a values are also accurately modeled using the second coupling picture. As the bright state level tunes over the energy of one of the dark states, the doublets first increase in splitting as the bright and dark states approach each other, then decrease as the states diverge. The plot of splitting versus energy produces an inverted parabola. The intensities of the doublet partners once again remain nearly equal until the bright and dark state levels are nearly degenerate.

When the energy of the bright state level is exactly degenerate with a dark state the splitting is unique. One transition is much more intense than the other three. Two of the remaining transitions are of equal intensity, being comprised of what was one of the intense doublets and one of the two small satellite peaks. The remaining transition is still weak and remains within the baseline noise. This degenerate situation would produce a triplet in the experimental spectrum located at the frequency of the calculated bright state transition. The triplet should occur in the vicinity of large doublet splittings, since the doublet splitting increases as the bright and dark state levels approach each other. The few triplets observed in our DFE experimental spectrum occur near large doublet splittings, at what is the crest of an inverted parabolic pattern.

The vibrational mode coupling picture with non-degenerate symmetric and antisymmetric dark states accounts for not only the general experimental doublet splitting patterns but also the intensity patterns. Further evidence of the accuracy of the model is found in the predictions of the triplet locations observed in the experimental spectrum of DFE. We conclude that the C-H stretch of DFE is coupled to a single dark vibration which contains enough torsional quanta to split its symmetric and antisymmetric dark states by more than our spectral resolution.

Computational Methods

A theoretical model was implemented to simulate vibrational mode coupling from a degenerate bright state to a split dark state in

an effort to reproduce more precisely the splitting and intensity patterns found experimentally in the DFE spectrum. Within this model, the bright states are not allowed to interact with each other nor are the dark states. One bright state couples strictly with the lower energy dark state while the remaining bright state couples strictly with the higher energy dark state. The Hamiltonian of this model reduces to two independent 2 x 2 matrices. The diagonal components of each matrix include one dark state and one bright state frequency and the off-diagonal terms are the coupling elements between the given bright and dark states. Diagonalization of these two matrices yields the positions for the four corresponding eigenstates. The peak intensities were calculated as specified in reference 36.

The spacing of the symmetric and antisymmetric dark states was varied as was the coupling matrix element in an effort to reproduce the experimental doublet splitting patterns. Shown in Figure 10 is the calculated and experimental splitting patterns for K_a=0. The calculated curve in Figure 10 used a coupling matrix element of 0.055 cm^{-1}, a dark state separation of 28.6 cm^{-1} and a lower energy symmetric dark state 1.9 ± 0.3 cm^{-1} below the excited 0_{00} rotational state. The error bars on the plot represent the 0.0004 cm^{-1} experimental resolution of our spectrum. The initial slope of the calculated curve is largely dependent upon the coupling matrix element and adequately fits the experimental data points. Towards the minimum of the calculated curve, where the bright state energy level is further from the dark state, the magnitude of the dark state

separation becomes more critical. The calculated fit is less accurate in this region. The width of the dark state spacing for the K_a=0 fit was defined largely from information obtained in fitting the K_a= 1 doublets and will be discussed in more detail in the next section. Two of the experimental data points display large deviations that are not predicted by the model. This anomalous behavior is not currently understood. The K_a=1 doublets have two different splitting patterns depending on the value of K_c in the excited state. Shown in Figure 11 is a plot of the experimental doublet splittings for the two K_a=1 Q-branch progressions as well as the calculated fits to each pattern. For both fits the dark states were separated by 25 cm^{-1} and the symmetric dark state was located 0.1 ± 0.5 cm^{-1} below the excited 0_{00} rotational state. The coupling matrix element is 0.055 cm^{-1} for the pattern where K_c=(J-K_a) and 0.07 cm^{-1} for K_c=(J-K_a+1). The splitting patterns for the remaining K_a progressions have not been reproduced at this point.

Discussion

Analysis of the rotationally resolved infrared spectrum of the C-H stretch in DFE suggests that vibrational mode coupling is the cause of the observed spectral fine structure. Other features of the DFE spectrum provide additional information about the potential surface of this molecule. In particular, we will address the following points: the K_a dependence in the doublet splitting patterns; the identity of the coupled dark state; the coupling mechanism; and the implications of the vibrational mode coupling for both the molecular structure and the photoisomerization reaction of DFE.

K_a Splitting Dependence

Insight into the K_a dependence in the doublet splitting patterns is obtained by examining the effects of molecular rotation on the torsional potential. DFE is a near symmetric top with $\kappa = -0.905$. Thus, the K_a quantum number has physical significance as a nearly good quantum number. The molecular A-axis lies nearly coincident with the C-C bond in DFE. Therefore, increased values of K_a correspond largely to an increase in rotation about the C-C bond. The effects of centrifugal distortion would cause the substituents on opposite carbons to become closer together with increased K_a values. As the two fluorines get closer the increased F--F interaction would produce an increase in the gauche-gauche rotational barrier, corresponding to a decrease in tunneling splitting in the torsional energy levels. Therefore, an increase in K_a would cause a decrease in symmetric and antisymmetric dark state spacing, manifested as an increase in the energy of the symmetric state and a decrease in energy of the antisymmetric state.

The change in energy of the dark states due to A-axis centrifugal distortion can be observed in the spectrum of DFE. The doublet splitting pattern for K_a=0 indicates that the symmetric dark state is 1.9 ± 0.3 cm^{-1} below the 0_{00} excited rotational state, as described above. When K_a=1 the symmetric dark state is located 0.1 ± 0.5 cm^{-1} below the 0_{00} excited rotational state. The few triplets assigned in the experimental spectrum have K_a=2 and are found where the doublet splitting appears to be at a maximum, the point

where the bright state becomes degenerate with a dark state, as expected. The location of the triplets indicate that the symmetric dark state is approximately 8.3 cm^{-1} higher in energy than the 0_{00} excited state for K_a=2. Triplets also indicate that the energy of the antisymmetric dark state is 13.1 cm^{-1} higher in energy than the 0_{00} excited bright rotational state for K_a=2. The K_a=3 progression similarly appears to represent a bright state tuning over the symmetric dark state. At K_a=3, the symmetric dark state is approximately 17 cm^{-1} higher in energy than the 0_{00} excited rotational state. In these doublet progressions, the energy of the symmetric dark state increases as a function of K_a. This observation is consistent with a decrease in the tunneling splitting as a function of A-axis rotation. As the dark state tunneling splitting becomes smaller, the tuning of the bright state energy samples more of the energy below and above the two dark states and less of the energy between them. As a result, the doublet splitting patterns for higher K_a's reveal an inverted parabolic behavior as the bright state approaches both dark states and then tunes beyond both dark states. Thus, the experimental data supports the conclusion that centrifugal distortion is responsible for the K_a dependence in the splitting patterns.

The 1.8 ± 0.8 cm^{-1} change in symmetric dark state energy was used to determine the dark state spacing for the K_a=0 splitting patterns. The increase in symmetric state energy is expected to be the same as the decrease in dark state energy because tunneling splitting is symmetric about the unperturbed K_a=0 energy level. The

dark state tunneling splitting was determined to be 25 cm^{-1} for the K_a=1 progressions from the experimental doublet splittings. Therefore, the splitting for the K_a=0 dark states was concluded to be 28.6 cm^{-1}. This is the splitting used in fitting the splitting patterns for Ka=0.

Identification of the Coupled Dark State

The doublets in the rotational fine structure indicate that the C-H stretch is coupled to a single dark vibration. In identifying the particular dark vibration coupled to the C-H stretch, three criteria must be met. First, the vibrational symmetry of the dark mode must be identical to that of the C-H stretch. DFE belongs to the C_2 point group which contains only two symmetry classes, A and B, with the C-H stretch being B-type. Therefore, the coupled dark mode must also be of B-type symmetry. Second, the dark vibration must contain enough torsional quanta to account for the 28.6 cm^{-1} spacing between symmetric and antisymmetric states for K_a=0. Finally, the symmetric state of the coupled dark vibration must lie approximately 1.9 cm^{-1} lower in energy than the excited 0_{00} rotational state as observed in the K_a=0 splitting progression. The 0_{00} rotational state energy corresponds to the center frequency of the C-H stretch band, 2986.44 cm^{-1}, placing the symmetric dark state at 2984.5 cm^{-1}. The identities and energies of the dark vibrational states neighboring the C-H stretch were determined using a simple state counting algorithm to see which states met these three requirements. Seventeen of the molecular vibrations were treated as oscillators with a 2% anharmonicity and the 18th vibration, the C-C

torsion was treated as a hindered rotor. The fundamental frequencies for the 17 oscillators were taken from reference 15. The torsional potential used in the hindered rotor calculation is the potential given in Eq.1. By using this Fourier potential in the state counting calculation, the torsional coordinate is treated as independent of the other vibrations in the molecule. The Fourier potential produces a 24 cm^{-1} tunneling splitting between the 15th and 16th energy levels, suggesting that the symmetric dark state must contain 15 quanta of C-C torsion. 373 vibrational states were found in the 2965-3000 cm^{-1} frequency region, corresponding to a density of 11 states/cm^{-1}. Of these states, only one came close to meeting the three criteria for the coupled dark vibrational mode. This state is composed of 1 quantum of CH_2 rock (B-type symmetry), 4 quanta of CCF bend (A-type symmetry) and 15 quanta of C-C torsion (A-type symmetry), and has an energy of 2985.87 cm^{-1}. Similar calculations were done using 0% and 4% anharmonicity in the 17 oscillator vibrations. The calculation with 0% and 4% anharmonicity produced no states which reasonably met all three requirements for the coupled dark state.

Vibrational Coupling Mechanism

The spectrum provides insight into the mechanism by which the bright and dark states are coupled. There are at least two coupling mechanisms present. The dominant mechanism is anharmonic coupling. Anharmonic coupling is evident in the fact that the 0_{00} excited rotational state is split by 0.00182 cm^{-1}. A rotationally dependent coupling mechanism would not cause coupling

in the 0_{00} rotational state. Anharmonic coupling is further confirmed in that each bright rotational state is coupled to only one rotational state in the symmetric and antisymmetric dark vibrations.

The second coupling mechanism is a rotation-vibration mechanism. The experimental spectrum has evidence of a minor component of Coriolis coupling in the B/C plane of DFE. The calculated fits to the two experimental splitting patterns where $K_a = 1$ required identical parameters except for coupling matrix elements. The data for $K_a=1$, $K_c=(J-K_a)$ are fit with the same coupling matrix element as the data for $K_a=0$, $K_c=(J-K_a)$, indicating the lack of significant A-axis Coriolis coupling. In contrast, the data for $K_a=1$, $K_c=(J-K_a+1)$ requires a larger coupling matrix element in calculating a fit to the doublet splitting pattern. Assuming that J is a good quantum number and K_a is nearly a good quantum number, the increase in coupling matrix element corresponds to a reorientation of a small component of angular momentum in the molecular B/C plane. With these observations, the increased coupling matrix element must be due to a Coriolis-type coupling in the B/C plane. Such Coriolis coupling must generate different coupling matrix elements for each doublet within any given doublet progression. The fact that the $K_a = 1$ data is fit well when Coriolis effects are neglected suggests that the B/C Coriolis coupling is a secondary perturbation.

Molecular Structure and Photoisomerization

A comparison of DFE and 2-fluoroethanol (2FE) is useful to better understand the ramifications of vibrational mode-coupling in molecular structure and photoisomerization dynamics. In both molecules, high resolution spectroscopy demonstrates that the C-H stretch is coupled to the C-C torsion coordinate. The average coupling matrix element in 2FE is 0.003 cm^{-1}, as compared to the matrix element for DFE, measured in the present study to be 0.055 cm^{-1}. In 2FE the bright state couples to numerous other dark states and as a result, the coupling matrix element varies from 0.0004 to 0.009 cm^{-1} depending on the identity of the dark state. The difference in the magnitude of the coupling could result from the difference in the nature of the physical interactions which stabilize the gauche conformer in the two molecules. In 2FE, the gauche stabilization is the result of an attractive interaction between the C-F bond dipole and the O-H bond dipole, which are nearly anti-parallel. In DFE the gauche stabilization is caused by a gauche effect which is much weaker. In 2FE the bond-dipole attractive interactions could restrict the torsional motion, making it less available to couple to the C-H stretch. The relative energies of the gauche and trans conformers have proven difficult to measure accurately by experiment, particularly in the gas phase. One exception is a gas phase NMR measurement of 280 cm^{-1} for the energy difference for DFE conformers.[20] High level ab initio calculations are in reasonable agreement with this value for DFE (224-273 cm^{-1})[7] and predict an energy difference of 710-784 cm^{-1} for 2FE[37].

Both DFE and 2FE have been observed to photoisomerize in low temperature matrices. A great deal of interest has focused on the role of vibrational mode-coupling in the photoisomerization of both molecules. Mode-selective vibrational coupling to the reactive coordinate has been proposed to be an important component of the reactive mechanism for photoisomerization in 2FE.[29] The larger coupling present in DFE could be manifested in the reaction rate for photoisomerization. It is important to examine, however, the nature of the dark states participating in the mode-coupling. In 2FE, many of the numerous dark vibrational modes coupled to the bright state have enough torsional quanta to be above the barrier to conformational isomerization. In contrast, the dark state coupled to the C-H stretch in DFE contains 15-16 torsional quanta, placing the dark state 100 cm^{-1} below the top of the gauche-trans potential barrier. Nevertheless, it is possible that vibrational mode coupling plays a role in the photoisomerization of DFE. Comparison of the relative reaction rates for photoisomerization of 2FE and DFE are virtually impossible because the literature matrix studies for the two molecules have been performed under very different experimental conditions. Careful examination of the photoisomerization of 2FE and DFE under the same conditions in low temperature matrices would be invaluable in determining the relationship between mode-selective vibrational mode-coupling and photoisomerization reaction rates.

Conclusions

High resolution infrared spectroscopy of DFE has presented some valuable insights into the structure and dynamics of this simple organic molecule. Analysis of the rotational structure in the transition composed of the symmetric combination of asymmetric C-H stretches revealed that the equilibrium geometry for the excited vibration is very similar to the gauche ground state geometry. The rotational fine structure indicates that this C-H stretch is undergoing vibrational mode coupling to a combination mode containing many quanta of torsional energy. The combination mode is split into distinct symmetric and antisymmetric energy levels as a result of tunneling between the two gauche conformers of DFE. From the rotational fine structure in the spectrum it was possible to determine the identity of the dark state. The nature of the coupling between the C-H stretch and the symmetric and antisymmetric combination modes appears to be largely anharmonic. A minor additional, rotationally dependent coupling was also detected. This minor coupling is suggested to be caused by Coriolis coupling in the molecular B/C plane.

The strength of the coupling between the C-H stretch and a highly excited torsional mode has implications for both the structure and dynamics. Compared to 2FE, the intramolecular attractive interactions which stabilize the gauche conformer are smaller in DFE. Concomitantly, the mode-coupling to the torsion is stronger. The correlation between stabilization energy and mode-coupling supports the idea that the attractive interactions hinder the mode-coupling by

locking the conformational structure in place. The comparison of the mode-coupling to the reaction rates for DFE and 2FE await further matrix experiments.

Acknowledgments

This work is supported by: The National Institute of Health under grant #08-R9N527039A; The Office of Naval Research under grant #N00014-90-J-1971; and The Petroleum Research Fund, administered by the American Chemical Society. The authors gratefully acknowledge the assistance of Christopher L. Brummel, and Julian M. Hjortshoj. The authors would also like to thank Prof. Kevin Lehmann and Erik Kerstel for helpful suggestions.

References

1. J. Kommandeur, W. A. Majewski, W. L. Meerts, D. W. Pratt, *Ann. Rev. Phys. Chem.*, **38**, 433 (1987).

2. A. M. de Souza, D. Kaur, D. S. Perry, *J. Chem. Phys.*, **88**, 4569 (1987); A. M de Souza, D. Kaur, D. S. Perry, *Ber. Buns. Phys. Chem.*, **92**, 424 (1988).

3. A. McIlroy, D. J. Nesbitt, *J. Chem. Phys.*, **92**, 2229 (1990); K. K. Lehmann, B. H. Pate, B. Scoles, unpublished results.

4. J. Go, G. A. Bethardy, D. S. Perry, *J. Chem. Phys.*, **94**, 6153 (1990).

5. C. L. Brummel, S. W. Mork, L. A. Philips, *J. Am. Chem. Soc.*, **113**, 4342 (1991).

6. C. L. Brummel, S. W. Mork, L. A. Philips, *J. Chem. Phys.*, **95**, 7041 (1991).

7. K. Wiberg, M. Murcko, K. Laidig, P. J. MacDougall, *J. Phys. Chem.*, **94**, 6956 (1990).

8. D. Dixon, B. Smart, *J. Phys. Chem.*, **92**, 2729 (1988).

9. L. Radom, J. Baker, P. Gill, R. Nobes, N. Riggs, *J. Mol. Struct.*, **126**, 271 (1986); R. Abraham, R. Stolevik, *Chem. Phys. Lett.*, **77**, 181 (1981); R. J Abraham, K. Parry, *J. Chem. Soc. (B).*, No. 3, 539 (1970).

10. L. Raff, *J. Chem. Phys.*, **89**, 5680 (1988); *J. Phys. Chem.*, **91**, 3266 (1987); T. Miyajima, Y. Kurita, T. Hirano, *J. Phys. Chem.*, **91**, 3954 (1987); K. Wiberg, M. Murcko, *J. Phys. Chem.*, **91**, 3616 (1987); G. Smits, M. Krol, P. Van Kampen, C. Altona, *J. Mol. Struct.* (Theochem), **139**, 247 (1986); L. Dosen-Micovic, D. Jeremic, N. Allinger, *J. Am. Chem. Soc.*, **105**, 1723 (1983); A. Kiss, A. Lopata, *J. Mol. Struct.*, **104**, 411 (1983); R. Boyd, L. Kesner, *J. Chem. Phys.*, **72**, 2179 (1980); K. Kveseth, *Acta Chem. Scand.*, **32A**, 51 (1978); A. Meyer, *J. Comp. Chem.*, **1**, 111 (1980); *J. Mol. Struct.*, **49**, 383 (1978); A. Meyer, N. Allinger, *Tetrahedron*, **31**, 1971 (1975); R. Abraham, P. Loftus, *J. Chem. Soc. Chem. Comm.*, **5**, 180 (1974); L. Radom, W. Lathan, W. Hehre, J. Pople, *J Am. Chem. Soc.*, **95**, 693 (1973); T. K. Ha, Hs. H. Günthard, *Chem. Phys.*, **134**, 203 (1989).

11. L. Radom, P. Stiles, M. Vincent, *J. Mol. Struct.*, **48**, 431 (1978); W. Reynolds, D. Wood, *Can. J. Chem.*, **51**, 2659 (1973).

12. M. Saunders, G. Webb, M. Tute, *J. Mol. Struct.*, **158**, 69 (1987); J. Rivail, D. Rinaldi, *Chem. Phys.*, **18**, 233 (1976).

13. Hs. H. Günthard, T. Ha, R. Gunde, *J. Mol. Struct.*, **217**, 143 (1990); R. Gunde, T. Ha, Hs. H. Günthard, *Chem. Phys.*, **145**, 37 (1990); R. Gunde, Hs. H. Günthard, *Chem. Phys.*, **126**, 229 (1988); *Chem. Phys.*,**111**, 339 (1987); R. Gunde. P. Felder, Hs. H. Günthard, *Chem. Phys.*, **64**, 313 (1982).

14. L. M. Raff, R. W. Graham, *J. Phys. Chem.*, **92**, 511 (1988); L. M. Raff, *J. Chem. Phys.*, **89**, 5680 (1988); *J. Chem. Phys.*, **90**, 6313 (1989); H. W. Schranz, L. M. Raff, D. L. Thompson, *Chem. Phys. Lett.*, **182**, 455 (1991).

15. W. Harris, J.Holtzclaw, V. Kalasinsky, *J. Chem. Phys.*, **67**,3330 (1977).

16. H. Takeo, C. Matsumura, Y. Morino, *J. Chem. Phys.*, **84**, 4205 (1986).

17. H. Dreizler, D. Steffek, *Z. Naturforsch*, **36A**, 1239 (1981).

18. S. Butcher, R. Cohen, T. Rounds, *Chem. Phys.*, **54**, 4123 (1971).

19. Hs. H. Günthard, *J. Mol. Struct.*, **113**, 141 (1984); P. Felder, Hs. H. Günthard, *Chem. Phys.*, **71**, 9 (1982).

20. T. Hirano, S. Nonoyama, T. Miyajima, Y. Kurita, T. Kawamura, H. Sato, *J. Chem. Soc. Chem. Comm.*, No. 8, 606 (1986).

21. P. Klaboe, J. Nielsen, *J. Chem. Phys.*, **33**, 1764 (1960); R. Abraham, R. Kemp, *J. Chem. Soc. B*, No. 6, 1240 (1971).

22. D. Friesen, K. Hedberg, *J. Am. Chem. Soc.*, **102**, 3987 (1980); B. Beagley, D. Brown, *J. Mol. Struct.*, **54**, 175 (1979); E. Van Schaick, H. Geise, F. Mijlhoff, G. Renes, *J. Mol. Struct.*, **16**, 23 (1973).

23. P. Felder, Hs. H. Günthard, Chem. *Phys. Lett.*, **66**, 283 (1979); *J. Mol. Struct.*, **60**, 297 (1980); *J. Mol. Spect.*, **95**, 68(1982); *Chem Phys. Lett.*, **88**, 473 (1982); *Chem. Phys. Lett.*, **85**, 1 (1984). P. Huber-Wälchli, Hs. H. Günthard, *Chem. Phys. Lett.*, **30**, 347 (1975); *Spectrochimica Acta*, **37A**, 285 (1981); M. Dubs, Hs. H. Günthard, *Chem. Phys. Lett.*, **64**, 105 (1979); *J. Mol. Struct.*, **60**, 311 (1980); M. Dubs, L. Ermanni, Hs. H. Günthard, *J. Mol. Spect.*, **91**, 458 (1982).

24. L. Fernholt, K. Kveseth, *Acta Chem. Scand. A*, **34**, 163 (1980).

25. San-Ichiro Mizushima, Structure of Molecules and Internal Rotation, Academic Press Inc., New York, 1954.

26. R. C. Bingham, *J. Am. Chem. Soc.*, **98**, 535 (1976); N. D. Epiotis, S. Sarkanen, D. Bjorkquist, L. Bjorkquist, and R. Yates, *J. Am Chem. Soc.*, **96** 4075 (1974); T. C. Brunck, F. Weinhold, *J. Am. Chem. Soc.*, **101**, 1700 (1979); S. Wolfe, *Accounts of Chem. Research*, **5**, 102 (1972); C. A. Kingsbury, *J. Chem. Ed.*, **56**, 431 (1979).

27. H. Frei, G. C. Pimentel, *Ann. Rev. Phys. Chem.*, **36**, 491 (1985).

28. J. Pourcin, M. Monnier, P. Verlaque, G. Davidovics, R. Lauricella, C. Colonna, H. Bodot, *J. Mol. Spect.*, **109**, 186 (1985).

29. W. F. Hoffman III, J. S. Shirk, *Chem. Phys.*, **78**, 331 (1983); Z. H. Kafafi, C. L. Marquardt, J. S. Shirk, *J. Chem. Phys.*, **90**, 3087 (1989); J. S. Shirk, C. L. Marquardt, *J. Chem. Phys.*, **92**, 7234 (1990); W. F. Hoffman III, J. S. Shirk, *J . Phys. Chem.*, **89**, 1715 (1985).

30. P. Buckley, P. A. Giguere, d. Yamamoto, *Can. J. Chem.*, **46**, 2917 (1968); M. Rasanen, J. Murto, V. E. Bondybey, *J. Phys. Chem.*, **89**, 3967 (1985); J. Pourcin, B. Davidovics, H. Bodot, L. Abouaf-Marguin, B. Gauthier-Roy, *Chem. Phys. Lett.*, **74**, 147 (1980); M. Perttila, J Murto, A. Kivinen, *Spect. Acta*, **34A**, 9 (1978); O. Shrems, *Ber. Bunserges Phys. Chem.*, **89**, 297 (1985); M. Rasanen, H. Kunttu, J. Murto, *Laser Chem.*, **9**, 123 (1988).

31. Program writtten by A. Maki and furnished to us by G. T. Fraser, N.I.S.T., Gaithersberg, MD, 20899.

32. Average value of rotational constants taken from microwave values in references 16, 17, 18.

33. J. Hjortshøj and L. A. Philips, (*J. Mol. Spect.*, accepted).

34. A complete listing of assigned transitions may be obtained from PAPS.

35. The excited energy levels determined through exact diagonalization of asymmetric rotor Hamiltonian using program (asym82) written by A. Maki and furnished to us by G. T. Faser, N.I.S.T., Gaithersberg, MD, 20899. Ground state rotational constants taken from literature as cited in reference 32. Excited state rotational constants determined by simulated-annealing fit.

36. Eigenstate energies were determined through the diagonalization of a 2x2 Hamiltonian matrix with diagonal elements corresponding to bright and dark state frequencies and off diagonal elements corresponding to the coupling elements. The eigenstate transition intensities were normalized to unity and calculated as shown below:

$$\text{Int}(1) = \frac{(\text{Freq}(\text{bright state}) - \text{Freq}(\text{eigenstate}(2)))}{(\text{Freq}(\text{eigenstate}(1)) - \text{Freq}(\text{eigenstate}(2)))}$$

$$\text{Int}(2) = (1 - \text{Int}(1))$$

37. K. B. Wiberg, M. A. Murcko, *J. Mol. Spect.* (Theochem), **163**, 1 (1980).

Figure Captions

Figure (1)

The experimental spectrum and best calculated spectrum are shown as bar graph plots. Each bar corresponds to a frequency and intensity of a peak in the spectrum.

Figure (2)

a) A diagram representing the coupling between a degenerate bright rotational level and a degenerate dark rotational level is shown. The symmetric states are represented by black bars and the antisymmetric states are represented by striped bars. The coupling results in two doubly degenerate eigenstate levels.

b) A diagram representing the coupling between a degenerate bright rotational level and a non-degenerate dark rotational level is shown. Once again, the symmetric states are black and the antisymmetric states are striped. The coupling results in four rotational eigenstates, each of unique energy.

Figure (3)

A section of the Q-branch progression for K_a=0 is shown with a bar-graph plot of the calculated spectrum. Each transition in the calculated spectrum is labeled with quantum number assignments ($J_{Ka,Kc}$). Note the spacing of the experimental doublets decreases with increasing J, yet the intensities of the doublet partners remain nearly equal.

Figure (4)

The experimental doublet spacings are plotted as a function of the excited state rotational energy for the K_a=0 and K_a=1 progressions. Error bars represent the experimental 12 MHz spectral resolution. Note the initial decrease and subsequent increase in splitting as the excited rotational energy increases.

Figure (5)

A plot of the experimental doublet spacings versus excited state rotational energy is shown for the K_a=3,4,5 progressions. Error bars represent the experimental 12 MHz spectral resolution. Note the initial increase and subsequent decrease in splitting as the excited rotational energy increases, in contrast to Figure (4).

Figure (6)

Vibrational manifolds defined by different rotational constants, and therefore composed of rotational levels with different energy spacings, are shown diagrammatically in the figure. Rotational states with identical rotational quantum numbers in the two vibrations tune and detune with each other as one increases energy.

Figure (7)

Shown schematically are the expected splittings for three coupling scenarios using degenerate bright and dark rotational levels. Above are the relative spacings of the zeroth-order rotational levels and below are the expected spectral splittings. Striped bars represent antisymmetric states and solid bars represent symmetric states.

Figure (8)

Shown schematically are the expected splittings for five coupling scenarios using a degenerate bright level and non-degenerate dark rotational levels. Above are the relative zeroth-order state spacings and below are the expected spectral splittings. Striped bars represent antisymmetric states and solid bars represent symmetric states.

Figure (9)

A plot of the spacing of the "doublet" as a function of bright and dark state spacing. The plot is discontinuous when the bright state is degenerate with a dark state because at that point a triplet is formed with two peaks of identical intensity split by a single more intense peak. Striped bars represent antisymmetric states and solid bars represent symmetric states.

Figure (10)

The dots represent experimental doublets for K_a=0. The solid curve represents the expected splitting behavior assuming a coupling matrix element of 0.055 cm^{-1}, a dark symmetric and antisymmetric state spacing of 28.6 cm^{-1} and a symmetric dark state energy 1.9 cm^{-1} below the bright state 0_{00} energy.

Figure (11)

The squares represent experimental doublets for K_a=1. The solid curve represents the expected splitting behavior assuming a coupling matrix element of 0.055 cm^{-1}, a dark symmetric and antisymmetric spacing for 25 cm^{-1} and a symmetric dark state energy 0.1 cm^{-1} below the bright state 0_{00} energy. The dashed curve represents the expected splitting behavior assuming the same parameters as the solid curve except the coupling matrix element, which is 0.07 cm^{-1}.

Table Captions

Table (1)

The parameters for the best simulated-annealing fit to the experimental rotational contour using a rigid rotor model.

Table (2)

The first three columns present the rotational quantum numbers for the assigned excited state. The second column presents the average doublet splitting for transitions to that excited state. The last column indicates how many different assignments were made to that particular rotational state.

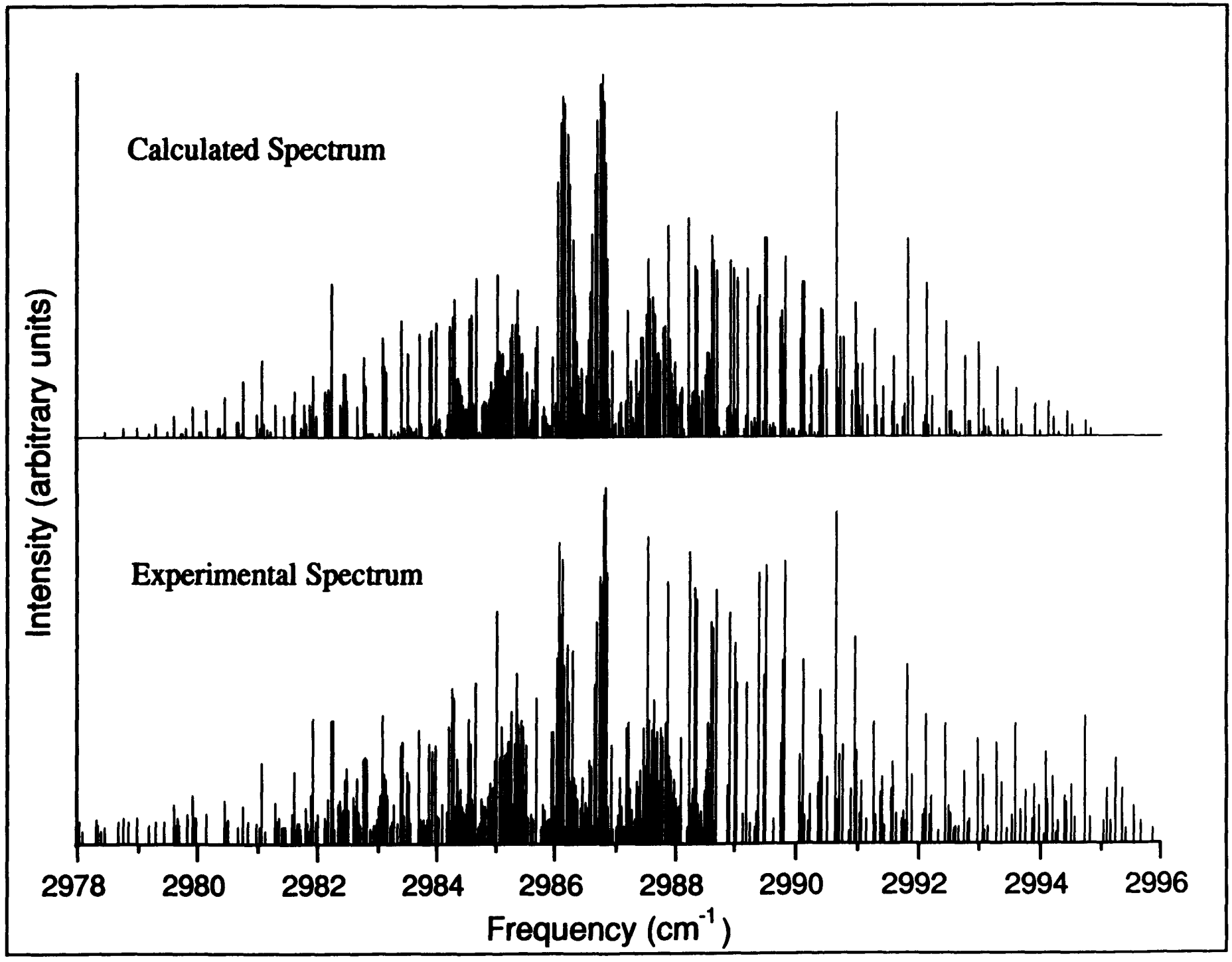
Calculated Spectrum
Experimental Spectrum
Intensity (arbitrary units)
2978
2980
2982
2984
2986
2988
2990
2992
2994
2996
Frequency (cm-1)

Dark Mode: No Torsion

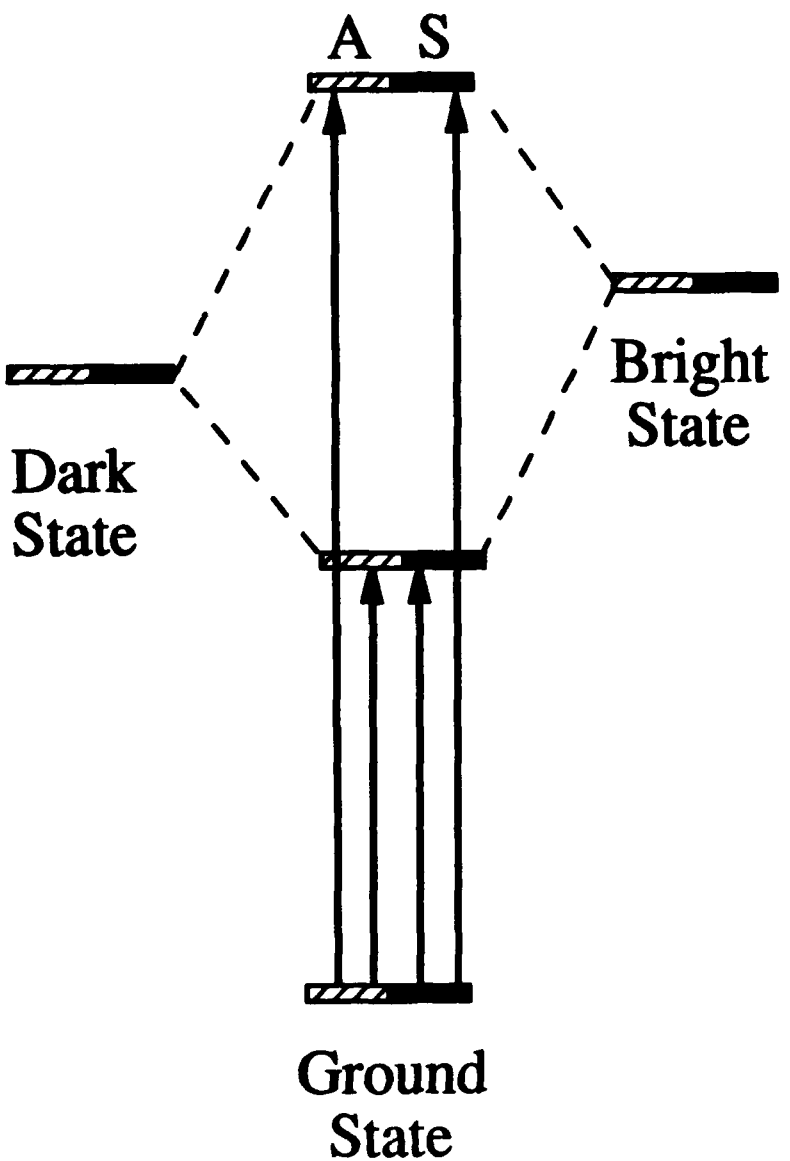

Dark Mode: Torsion

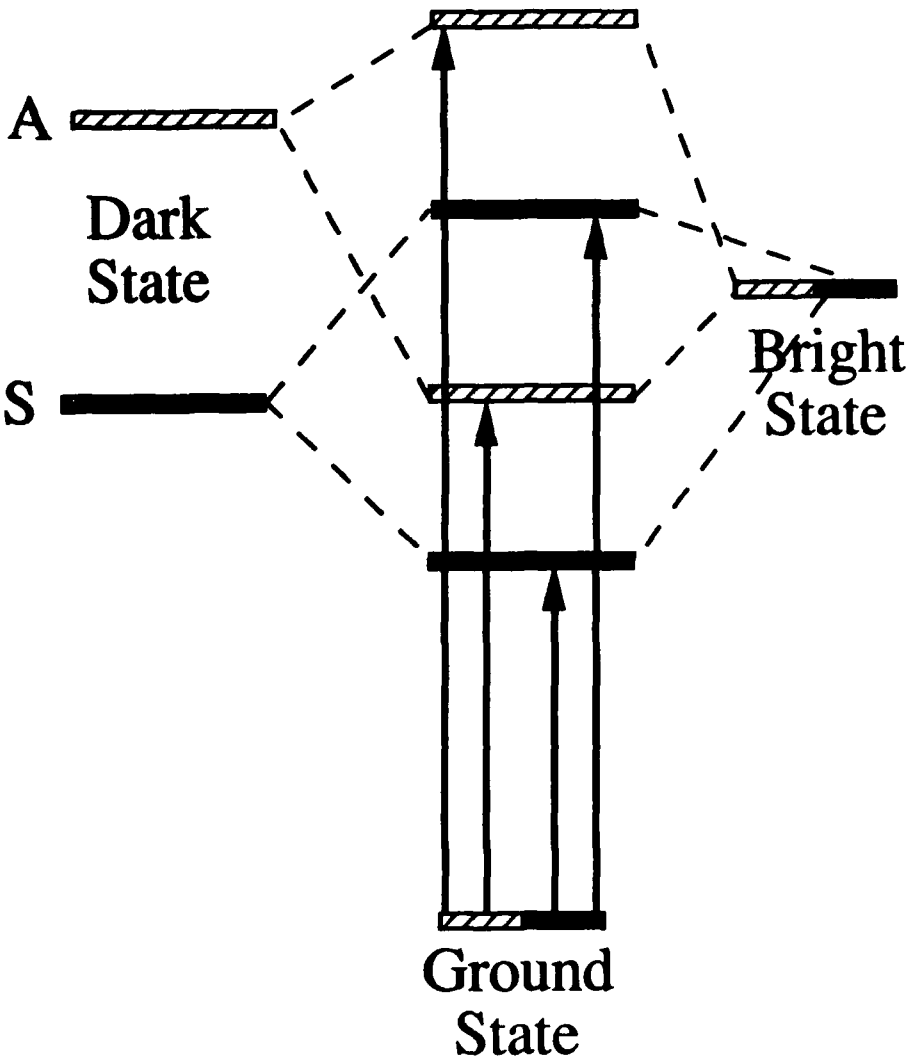

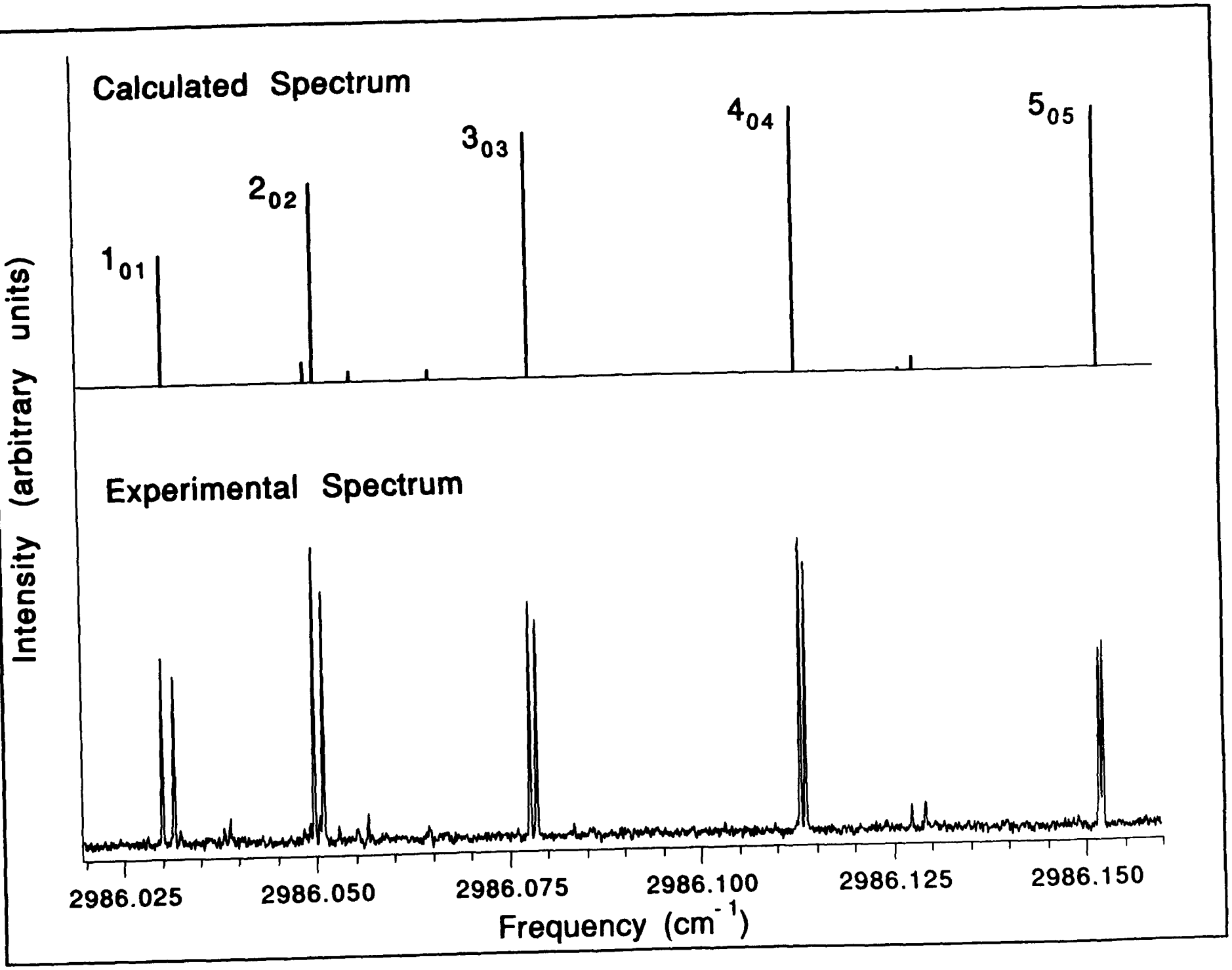
Calculated Spectrum
1_{01}
2_{02}
3_{03}
4_{04}
5_{05}
Experimental Spectrum
Intensity (arbitrary units)
2986.025
2986.050
2986.075
2986.100
2986.125
2986.150
Frequency (cm^{-1})

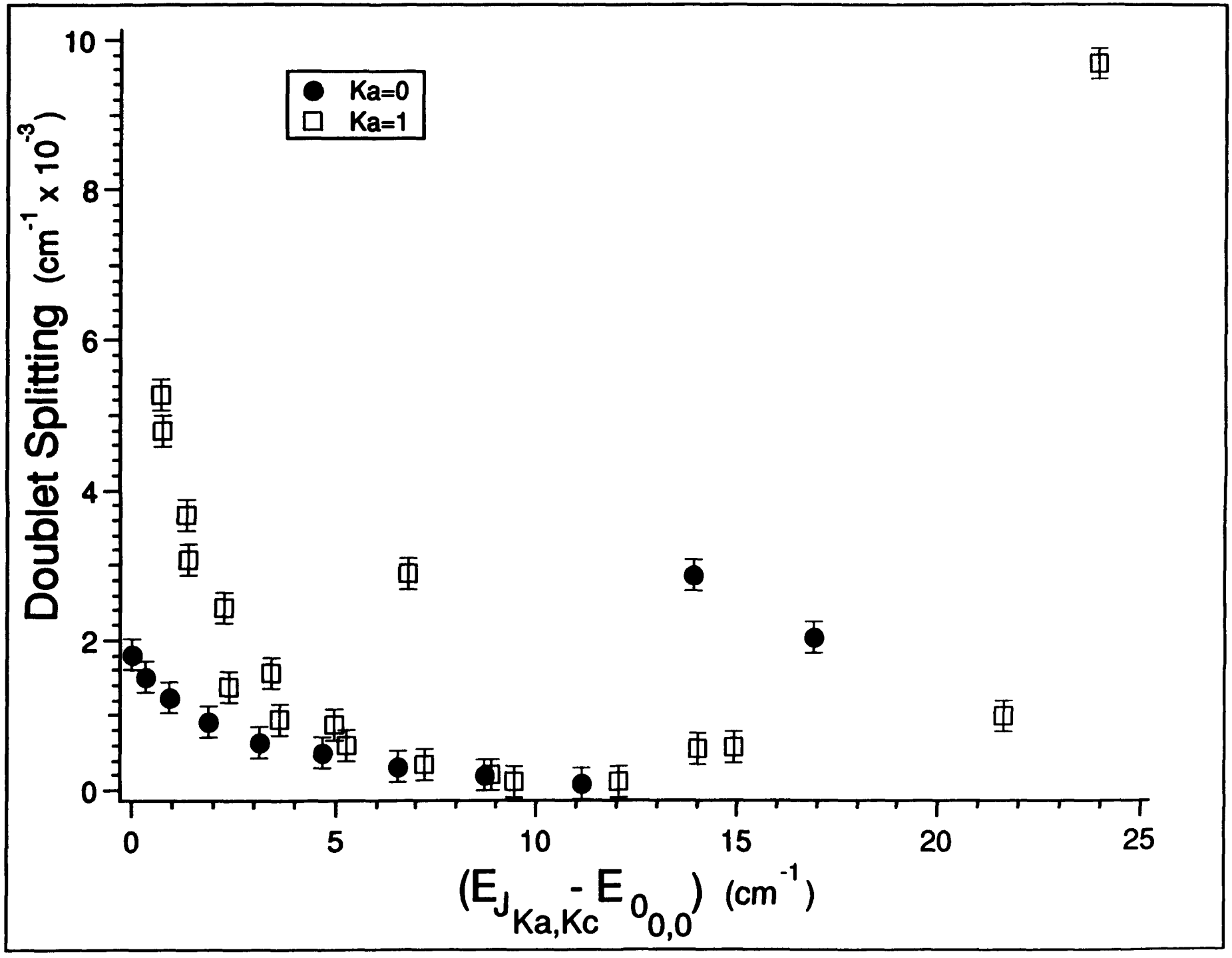
Ka=0
Ka=1
Doublet Splitting (cm-1 x 10-3)
(EJKa,Kc - E0 0,0) (cm-1)
0
2
4
6
8
10
0
5
10
15
20
25

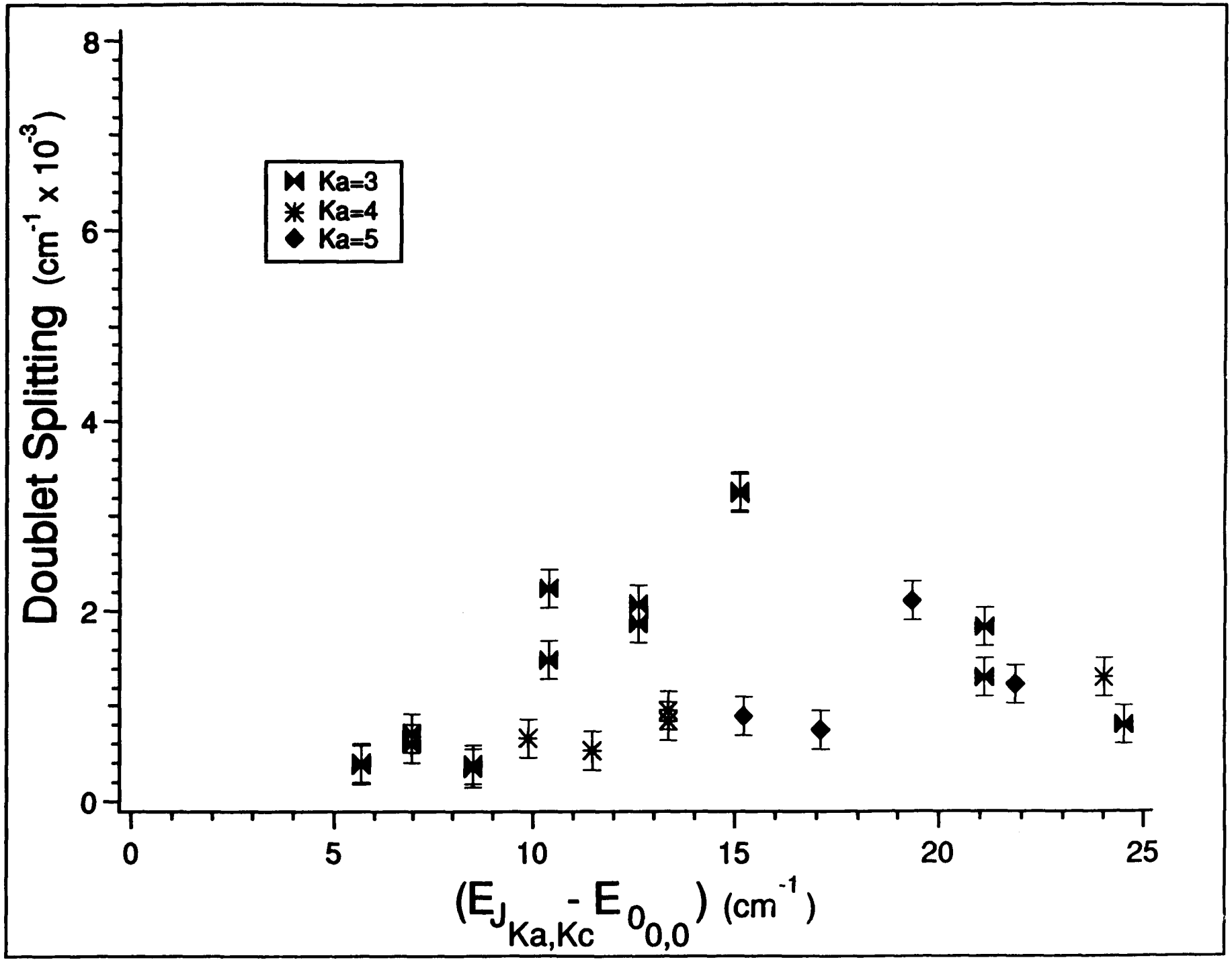
Ka=3
Ka=4
Ka=5
Doublet Splitting (cm-1 x 10-3)
0
2
4
6
8
0
5
10
15
20
25
(EJKa,Kc - E0 0,0) (cm-1)

Rotational Levels For Different Geometries

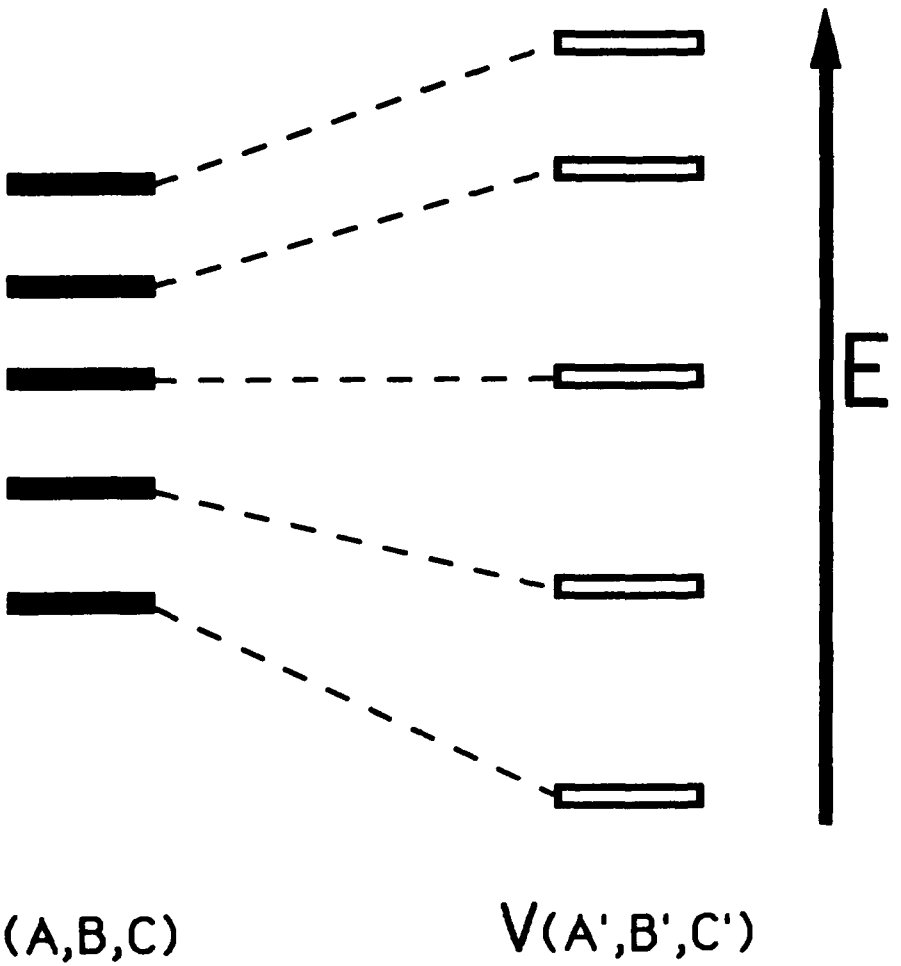

No Torsion in Dark State

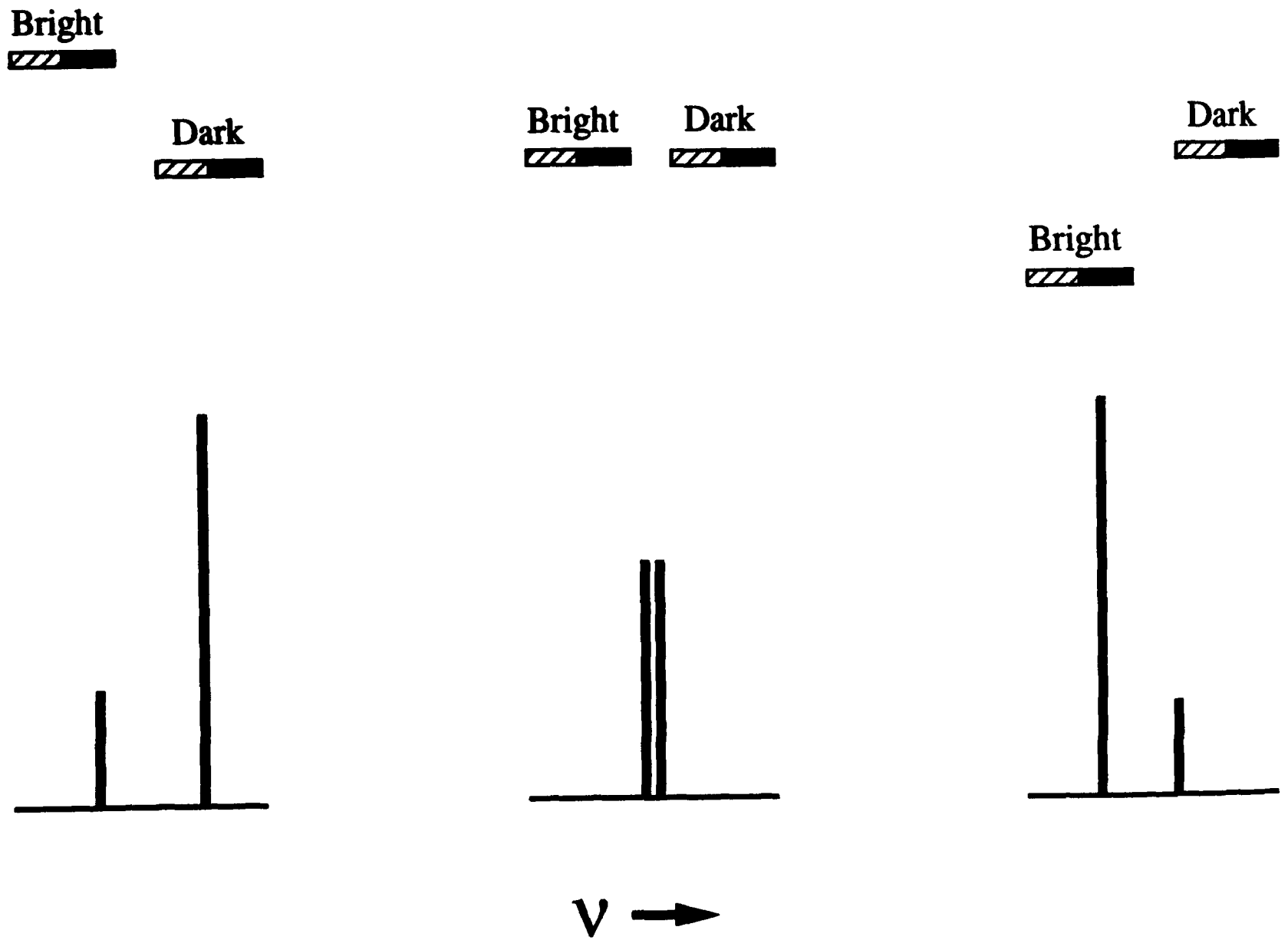

Torsion Present in Dark State

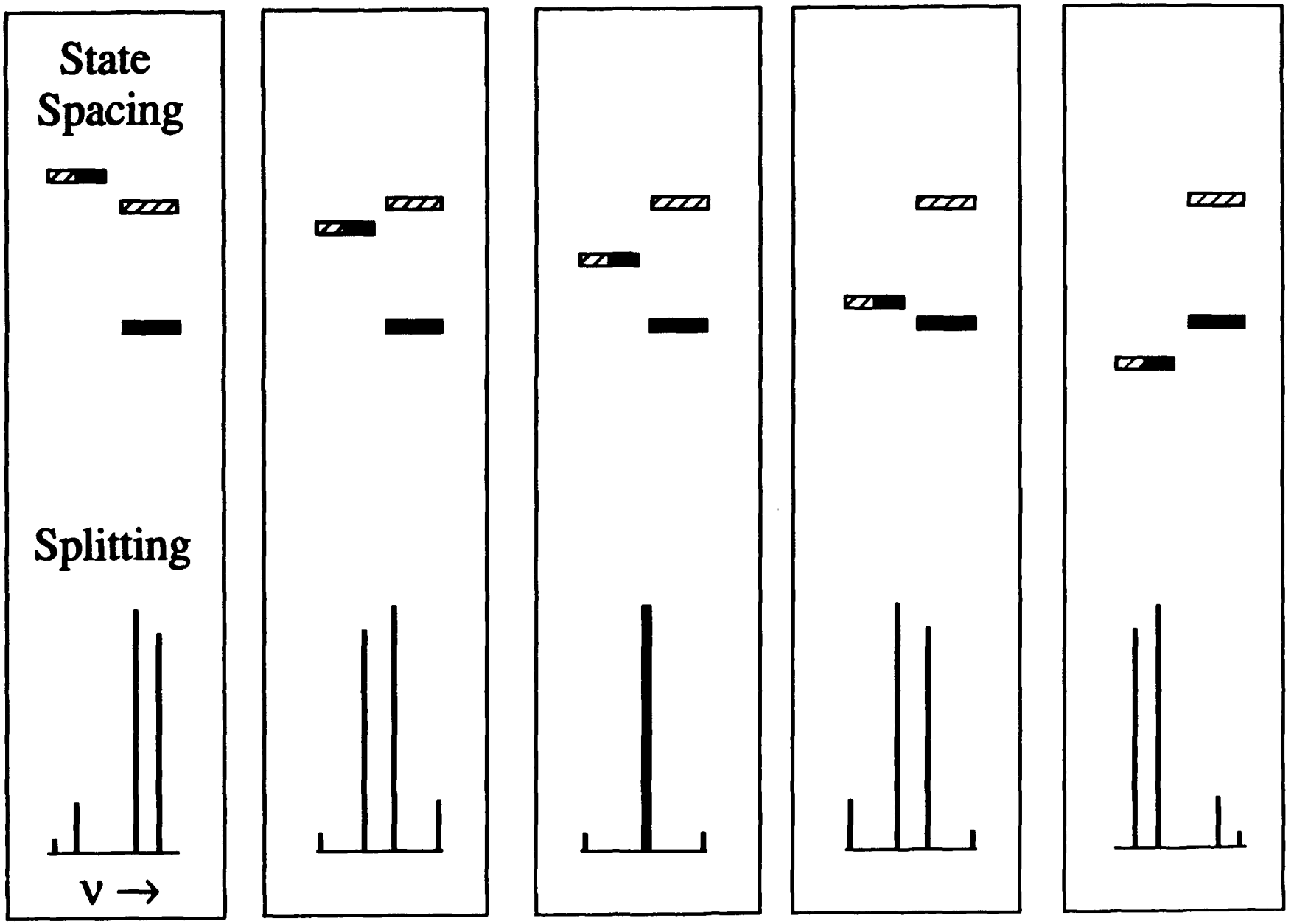

Doublet Splitting vs Bright and Dark State Spacing

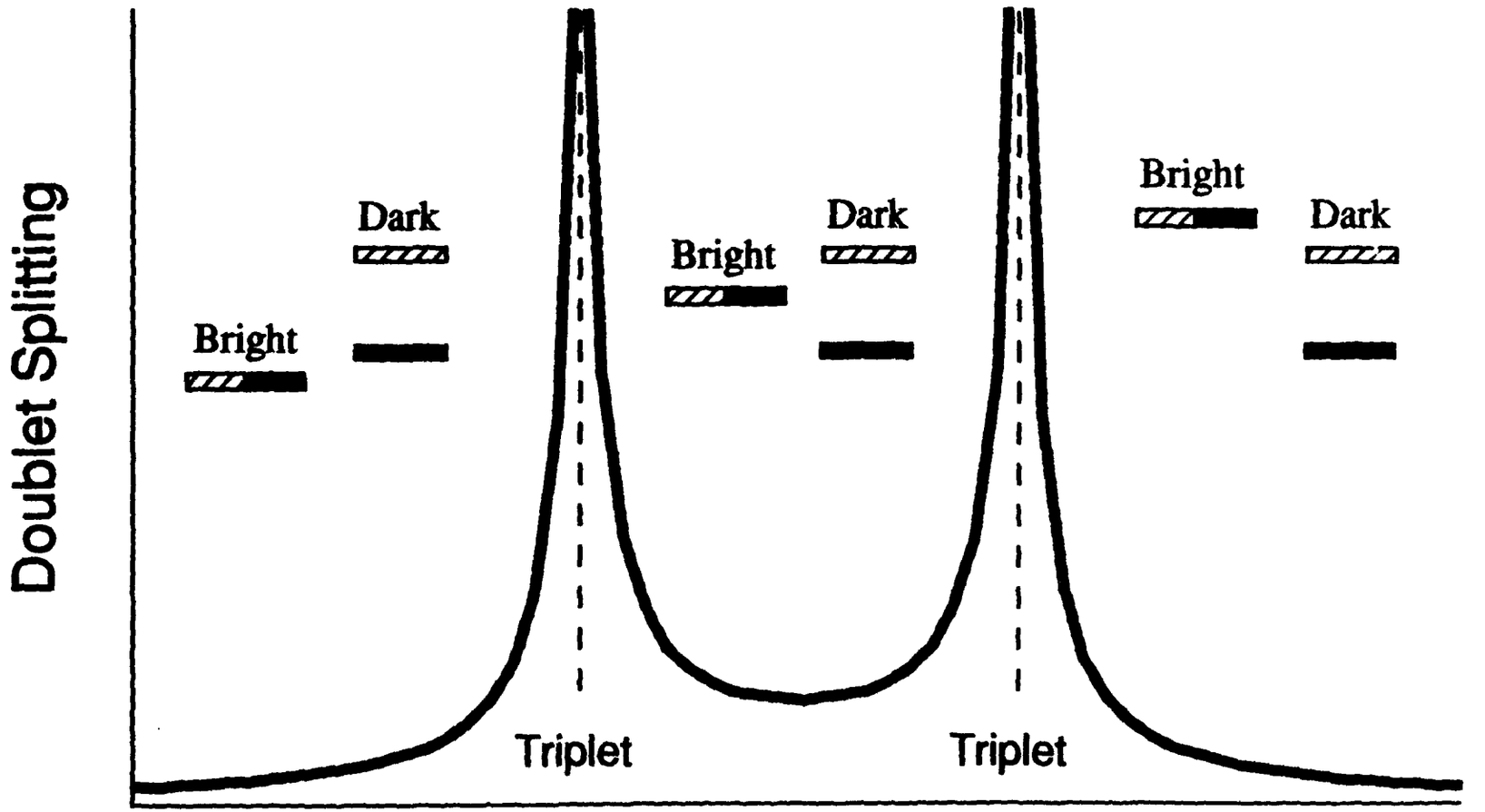

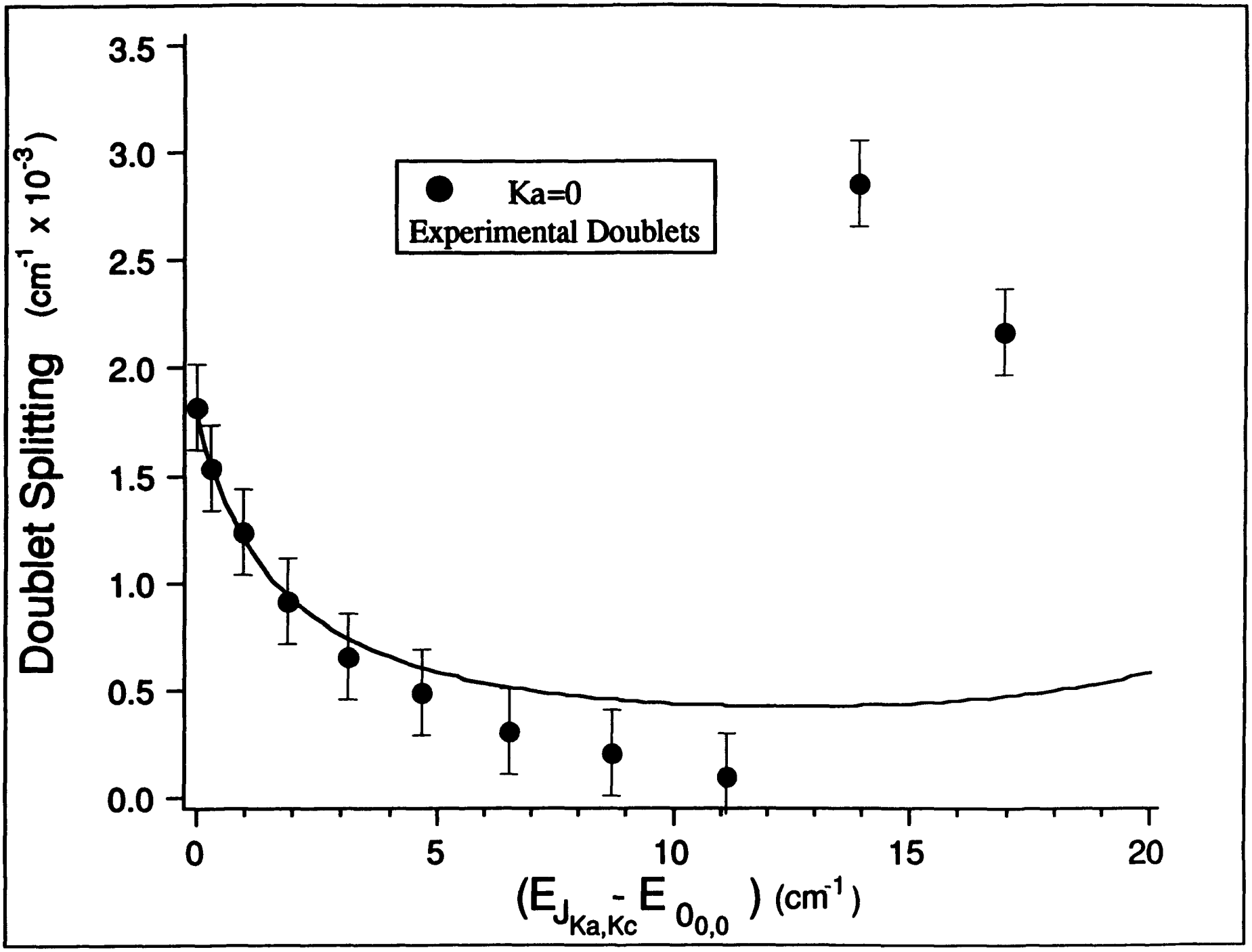
Ka=0
Experimental Doublets
Doublet Splitting (cm-1 x 10-3)
3.5
3.0
2.5
2.0
1.5
1.0
0.5
0.0
0
5
10
15
20
(EJKa,Kc - E0,0,0) (cm-1)

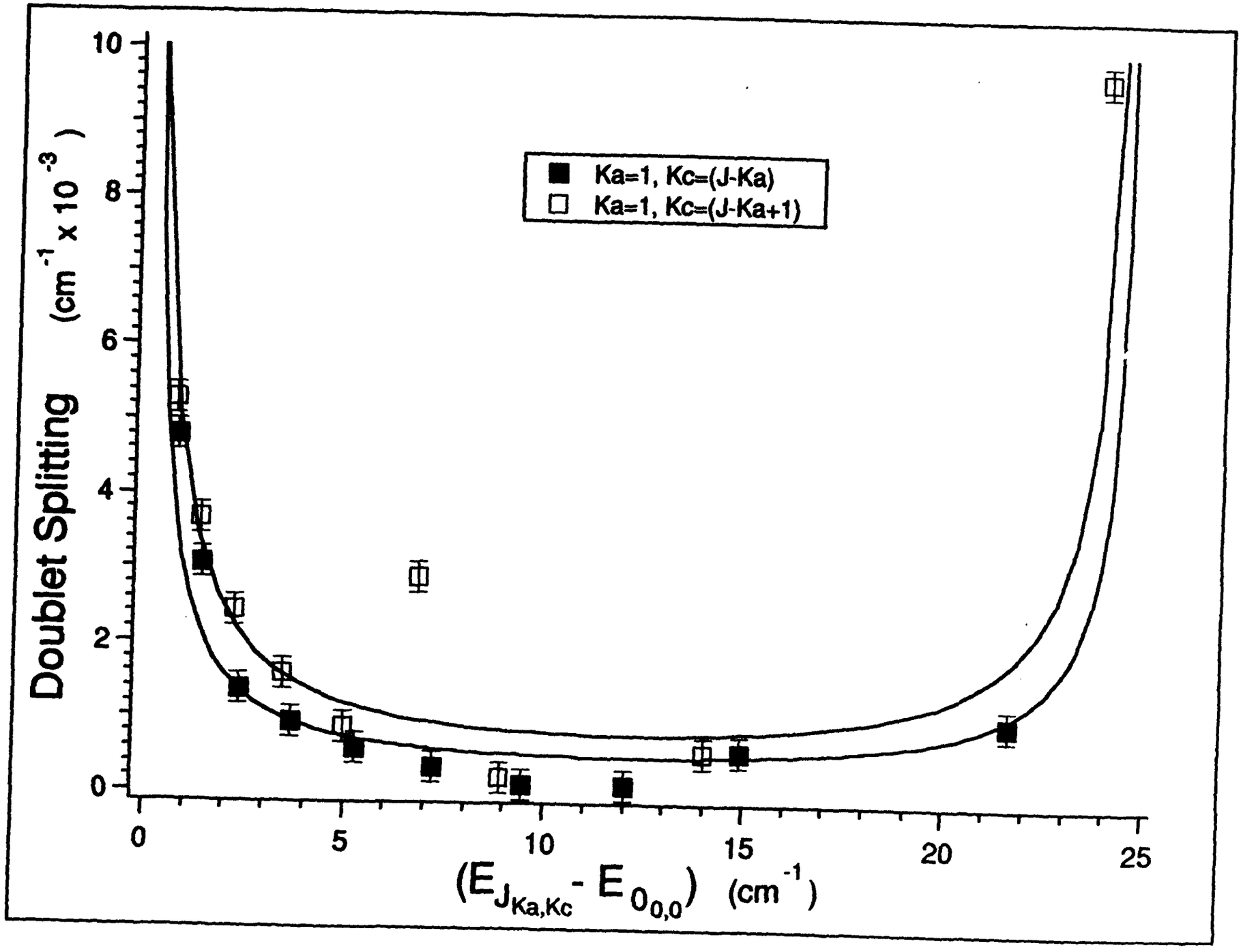
Doublet Splitting (cm^{-1} x 10^{-3})
10
8
6
4
2
0
0
5
10
15
20
25
(E$_{J_{Ka,Kc}}$ - E$_{0_{0,0}}$) (cm^{-1})
Ka=1, Kc=(J-Ka)
Ka=1, Kc=(J-Ka+1)

Calculated Fit Parameters

$A'' = 0.57781\ cm^{-1}$	$A' = 0.57779\ cm^{-1}$
$B'' = 0.16722$	$B' = 0.16690$
$C'' = 0.14619$	$C' = 0.14633$

$\mu_A = 0.3515$

$\mu_B = 0.9362$

$\mu_C = 0.0000$

$\nu_0 = 2986.44\ cm^{-1}$

$T = 8.1\ K$

J"	Ka"	Kc"	Average Splitting	N
0	0	0	0.0018	2
1	0	1	0.0015	4
1	1	0	0.0048	5
1	1	1	0.0053	4
2	0	2	0.0012	5
2	1	1	0.0031	7
2	1	2	0.0037	6
2	2	0	0.0026	4
2	2	1	0.0026	4
3	0	3	0.0009	5
3	1	2	0.0014	7
3	1	3	0.0024	6
3	2	1	0.0027	7
3	2	2	0.0025	5
3	3	0	0.0004	3
3	3	1	0.0004	4
4	0	4	0.0006	5
4	1	3	0.0009	7
4	1	4	0.0016	6
4	2	2	0.0013	8
4	2	3	0.0018	6
4	3	1	0.0006	3
4	3	2	0.0007	4
4	4	0	0.0007	3
4	4	1	0.0007	3
5	0	5	0.0005	5
5	1	4	0.0006	7
5	1	5	0.0009	6
5	2	3	0.0030	6
5	2	4	0.0061	4
5	3	2	0.0004	4
5	3	3	0.003	3
5	4	1	0.0005	2
5	4	2	0.0005	2
5	5	0	0.0009	3
5	5	1	0.0009	3
6	0	6	0.0003	4
6	1	5	0.0003	7
6	1	6	0.0029	3
6	2	4	--T--	5
6	2	5	--T--	3
6	3	3	0.0015	3
6	3	4	0.0022	3
6	4	2	0.0010	2
6	4	3	0.0008	2
6	5	1	0.0008	3
6	5	2	0.0008	3
7	0	7	0.0002*	2
7	1	6	0.0001*	7
7	1	7	0.0002	4
7	2	5	0.0002*	4
7	3	4	0.0019	2
7	3	5	0.0021	3
7	5	2	0.0021	3
7	5	3	0.0021	3
8	0	8	0.0001*	4
8	1	7	0.0001*	6
8	2	6	--T--	2
8	2	7	0.0032	3
8	3	5	0.0032	2
8	3	6	0.0033	2
8	5	3	0.0012	3
8	5	4	0.0012	3
9	0	9	0.0029	4
9	1	8	0.0006	5
9	1	9	0.0006	4
9	2	7	0.0008	2
9	2	8	0.0084	2
10	0	10	0.0020	3
10	3	7	0.0013	2
10	3	8	0.0018	2
10	4	7	0.0013	3
11	1	10	0.0010	3
11	3	9	0.0008	2
12	1	12	0.0097	2

* Indicates peaks appear as a singlet in the spectrum. Splitting was determined by using two gaussians, FWHM equal to that of a single peak of a doublet and finding the spacing required such that the FWHM of their sum equalled the FWHM of this singlet.

--T-- Indicates multiplet appears as a triplet.

TECHNICAL REPORT DISTRIBUTION LIST - GENERAL

Office of Naval Research (2)*
Chemistry Division, Code 1113
800 North Quincy Street
Arlington, Virginia 22217-5000

Dr. James S. Murday (1)
Chemistry Division, Code 6100
Naval Research Laboratory
Washington, D.C. 20375-5000

Dr. Robert Green, Director (1)
Chemistry Division, Code 385
Naval Air Weapons Center
Weapons Division
China Lake, CA 93555-6001

Dr. Elek Lindner (1)
Naval Command, Control and Ocean
Surveillance Center
RDT&E Division
San Diego, CA 92152-5000

Dr. Bernard E. Douda (1)
Crane Division
Naval Surface Warfare Center
Crane, Indiana 47522-5000

Dr. Richard W. Drisko (1)
Naval Civil Engineering
Laboratory
Code L52
Port Hueneme, CA 93043

Dr. Harold H. Singerman (1)
Naval Surface Warfare Center
Carderock Division Detachment
Annapolis, MD 21402-1198

Dr. Eugene C. Fischer (1)
Code 2840
Naval Surface Warfare Center
Carderock Division Detachment
Annapolis, MD 21402-1198

Defense Technical Information
Center (2)
Building 5, Cameron Station
Alexandria, VA 22314

* Number of copies to forward